

Effect of Earth-Moon's gravity on TianQin's range acceleration noiseXuefeng Zhang,^{1,*} Chengjian Luo,^{1,†} Lei Jiao,¹ Bobing Ye,¹ Huimin Yuan,¹ Lin Cai,^{2,‡}
Defeng Gu,¹ Jianwei Mei,¹ and Jun Luo^{1,2}¹*TianQin Research Center for Gravitational Physics & School of Physics and Astronomy,
Sun Yat-sen University (Zhuhai Campus), Zhuhai 519082, P. R. China*²*Center for Gravitational Experiments, School of Physics, MOE Key Laboratory of Fundamental Physical
Quantities Measurement & Hubei Key Laboratory of Gravitation and Quantum Physics, PGMF,
Huazhong University of Science and Technology, Wuhan 430074, P. R. China*

(Received 18 October 2020; accepted 8 February 2021; published 15 March 2021)

TianQin is a proposed space-borne gravitational-wave detection mission using circular high Earth orbits. The geocentric concept has raised questions about the disturbing effect of the nearby gravity field of the Earth-Moon system on the highly sensitive intersatellite ranging measurements. Here we examine the issue through high-precision numerical orbit simulations with detailed gravity-field models. By evaluating range accelerations between distant free-falling test masses, the study shows that the majority of the Earth-Moon's gravity disturbances are not in TianQin's detection frequency band above 10^{-4} Hz, and hence present no showstoppers to the mission.

DOI: [10.1103/PhysRevD.103.062001](https://doi.org/10.1103/PhysRevD.103.062001)**I. INTRODUCTION**

The current TianQin design assumes high Earth orbits with an orbital radius of 10^5 km [1]. The nearly equilateral-triangle constellation stands almost vertical to the ecliptic. High-precision laser-ranging interferometry tracks distance changes between well-protected test masses (TMs) in separate drag-free controlled satellites, within a preliminary frequency range of 10^{-4} –1 Hz. Proximity to the Earth has certain benefits, such as lower launch cost, shorter transfer duration, easier communication, availability of the Global Navigation Satellite Systems, etc. Other geocentric mission concepts [2] include OMEGA [3,4], GEOGRAWI/gLISA [5], GADFLI [6], B-DECIGO [7], etc. TianQin's orbit is different from these in both the orbital radius and orientation.

Space-based gravitational-wave (GW) detectors are subject to various influences from the surrounding environment, including gravity fields, thermal radiation, plasma, magnetic fields, solar-wind particles, galactic cosmic rays, micrometeorites, etc. that exist in outer space. Environmental effects can strongly affect the performance and lifetime of the spacecraft. Quite prominently, the space gravity-field environment—encompassing gravitational perturbations from the central and other celestial bodies—plays an important role. This is particularly true for geocentric missions due to their closeness to the Earth and Moon. More specifically, the effects on TianQin are twofold. On large scales, the perturbations distort the

nominal equilateral triangle of the constellation. The resulting unequal and time-varying arm lengths have far-reaching implications on science payload design and data-processing strategies (e.g., Refs. [8,9]). The distortion can be reduced by orbit optimization [10,11] and control to meet the stability requirements of the science payloads. On small scales, the perturbations impinge on TMs' geodesic motion under nearly pure gravity. Since space-based detectors accurately measure arm-length variations between TMs, they respond not only to GWs (radiation zone) but equally well to Newtonian gravity fields (near zone) in targeted frequency bands. Appearing as environmental noise, the latter should be avoided or mitigated.

Ideally, gravitational perturbations in space should only manifest as long-term and slow changes in interspacecraft displacement measurements. If there exists a proper separation in the frequencies of gravity-field fluctuations and GWs, then the GW signals—superimposed on top of a smooth and slowly varying background—can be extracted (see Sec 2.1.1 of Ref. [12]). Therefore, GW detection relies heavily on the “quietness” of the ambient gravity-field environment in the measurement band.

The problem of environmental gravity disturbances was recognized early on in designing ground-based detectors [13], and hence it is not unique to space missions, where the problem is thought to be much less severe. In ground-based detectors, Newtonian or gravity-gradient noise caused by terrestrial gravity fluctuations poses a limitation on sensitivity improvement below ~ 10 Hz [14]. Multiple strategies have been developed to effectively mitigate such noise, and the techniques have a major influence on designing next-generation ground-based detectors.

* zhangxf38@sysu.edu.cn

† luochj5@mail2.sysu.edu.cn

‡ cailin@hust.edu.cn

If not handled properly in space GW detection, disturbing gravity fields may induce excessive “orbital noise” that encroaches on the sensitivity curve, causing a situation somewhat similar to galactic foreground noise at lower frequencies [15]. The potential risk has drawn attention for TianQin, and may raise concern for other geocentric concepts as well. With regard to LISA [16], the majority of the effect is expected to be out of the sensitive frequency band because of its heliocentric yearly orbits and being placed far away from the Earth-Moon system ($\sim 20^\circ$ trailing angle, $\sim 5 \times 10^7$ km).

In general, gravity disturbances in space constitute an important potential noise source for interspacecraft measurements. In this work, we aim to determine the amplitudes and frequencies of the disturbances for TianQin’s orbit, and quantitatively evaluate the impact on TianQin’s acceleration noise requirement. The forward modeling takes into account a variety of main gravitational perturbations, including the gravity fields of the Earth (static and tidal), Moon, and Sun, as well as other Solar System bodies. It requires realistic and accurate orbit propagation that is also used in performance assessment and data analysis of gravity-mapping missions, such as GRACE [17], GRACE Follow-On [18], GOCE [19], and GRAIL [20]. However, for TianQin a problem with the insufficiency of double-precision arithmetic has emerged owing to the high measurement accuracy requirement over the long baseline. To tackle this issue, an earlier attempt was made in Ref. [21] where analytical expansions of perturbed orbits were derived. Unfortunately, the approach cannot handle complicated gravity field models, and only the Earth’s static gravity field was considered without a realistic model of Earth’s rotation (precession, nutation, etc.), the Earth’s tides, and third bodies. This motivated us to take a fully numerical approach, which we present in this paper. For other works regarding environmental magnetic and plasmic effects on TianQin, one can refer to, e.g., Refs. [22–24].

This is our third paper of the concept study series on TianQin’s orbit and constellation. It is based on the previous work of orbit optimization and constellation stability [10,11], and shifts the attention to small-scale orbital motion through much refined simulations. The paper is organized as follows. In Sec. II three types of intersatellite observables are analyzed, and the range acceleration is chosen for evaluating the impact. In Sec. III we describe the high-precision orbit propagator, detailed force models, and orbital parameters used in the assessment. Section IV presents the amplitude spectral density (ASD) results of the calculated range accelerations. Our conclusions are presented in Sec. V.

II. OBSERVABLES AND CRITERIA

For the purpose of evaluation, the numerical simulation should provide an observable accuracy better than the

instrumental measurement noise level. The selectable intersatellite observables include the (instantaneous) range, range rate, and range acceleration. Mathematically, they are interchangeable by differentiation and integration, but their numerical calculations require different computational resources. Here we estimate the magnitudes of their numerical ranges (numbers of significant digits required) for TianQin. First, the range between two satellites is given by

$$\rho = |\mathbf{r}_2 - \mathbf{r}_1|, \quad (1)$$

where $\mathbf{r}_{1,2}$ denotes the position vector of each satellite relative to the Earth’s center. Taking the baseline 1.7×10^8 m and the displacement measurement noise 1×10^{-12} m/Hz^{1/2} [1], the numerical representation of the range observable requires at least 20 digits, exceeding the 16 digits of the double-precision format (64 bits). Second, the range rate reads

$$\dot{\rho} = \hat{\mathbf{e}}_{12} \cdot (\dot{\mathbf{r}}_2 - \dot{\mathbf{r}}_1), \quad (2)$$

with the unit vector $\hat{\mathbf{e}}_{12} = (\mathbf{r}_2 - \mathbf{r}_1)/\rho$. The relative velocity between the TianQin satellites is expected to be within ± 5 m/s [10]. Taking the range-rate measurement noise 5×10^{-14} m/s/Hz^{1/2} ($\sim 2\pi f \times 10^{-12}$ m/Hz^{1/2} at the cross-over frequency $f \sim 10^{-2}$ Hz of the displacement and residual acceleration noises [1]), the dynamical range of $\dot{\rho}$ takes up about 15 digits. Third, differentiating the range rate yields the equation for the range acceleration:

$$\ddot{\rho} = \hat{\mathbf{e}}_{12} \cdot (\ddot{\mathbf{r}}_2 - \ddot{\mathbf{r}}_1) + \frac{1}{\rho} (|\dot{\mathbf{r}}_2 - \dot{\mathbf{r}}_1|^2 - \dot{\rho}^2), \quad (3)$$

where on the right-hand side the first term represents projected differential acceleration and the second term centrifugal acceleration. The gravitational acceleration of one TianQin satellite is on the order of 10^{-2} m/s². This is 13 orders of magnitude greater than the residual acceleration noise level of one TM, i.e., 1×10^{-15} m/s² [1]. For either $\dot{\rho}$ or $\ddot{\rho}$, if one takes into account that numerical errors compounded over time may occupy 2–3 digits, and redundant numerical accuracy another 1–2 digits, then the requirement would exceed 16 digits. Therefore, the commonly used double-precision arithmetic is insufficient in representing the intersatellite observables, and the associated roundoff error becomes a bottleneck for precision improvement (cf. Fig. 1).

Among the three observables, the range acceleration appears more favorable for taking up less digits in numerical computations. In the frequency domain, acceleration and displacement can be easily converted. For evaluating gravity disturbances in space, we henceforward adopt the range acceleration as the main observable (cf. [25]), and directly compare its ASD with the intersatellite residual acceleration noise requirement $\sqrt{2} \times 10^{-15}$ m/s²/Hz^{1/2} at 10^{-4} – 10^{-2} Hz as the criteria, which

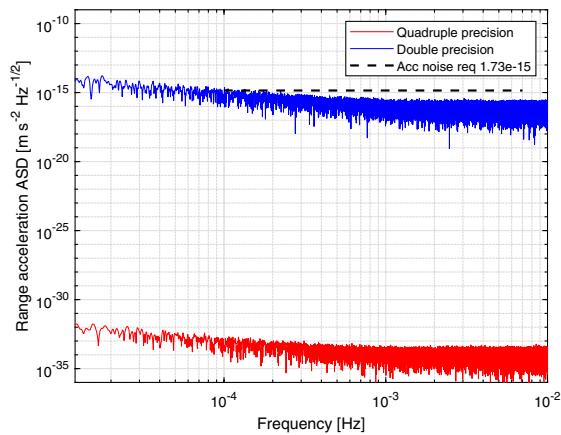


FIG. 1. ASD of the range acceleration $\ddot{\rho}$ between two satellites in circular orbits of radius 10^5 km and separated by 120° in phase. The orbits are integrated with a constant step size of 50 s and under the central force of the Earth's point mass. The roundoff error of the quadruple-precision arithmetic is at the level of 10^{-33} m/s²/Hz^{1/2} (at 10^{-4} Hz). The curve tilts up toward low frequencies due to the accumulation of roundoff errors over time. For comparison, the roundoff error of double precision is also shown, but at a much higher level of 10^{-15} m/s²/Hz^{1/2} (at 10^{-4} Hz), and hence not sufficient for the accuracy requirement.

is simply $\sqrt{2}$ of the residual acceleration noise of a single TM (cf. Ref. [26]). Note that this flat noise requirement is preliminary and expected to be relaxed near 10^{-4} Hz in the future [1,16].

III. SIMULATION AND FORCE MODELS

The evaluation requires careful calculation and modeling of satellite orbits and gravity fields. The accuracy of numerical integration must surpass the noise requirement $\sqrt{2} \times 10^{-15}$ m/s²/Hz^{1/2} of the range acceleration observable by at least 1 order of magnitude. The force modeling should be sufficiently detailed and up to date to reflect as many significant gravity disturbances as possible, particularly those that may enter the detection band.

A. Quadruple-precision orbit propagation

There exist a few strategies to tackle the inadequacy of double precision. A straightforward way is by extending to 34 significant digits with quadruple-precision arithmetic (128 bits). The potential downsides are low execution speed and heavy programming workload. Following this “brute force” approach, the TianQin Quadruple Precision Orbit Propagator program based on *Matlab* has been developed so as to evaluate the range acceleration at $< 10^{-15}$ m/s²/Hz^{1/2} levels. The quadruple-precision data type is applied to all of the necessary aspects of the program, including parameter inputs, ephemeris data outputs, reference frame transformations, time conversion, numerical integration, force models, etc. For the nearly circular high orbits, the integrator uses the

eighth-order embedded Prince-Dormand (DP87) method [27] with a constant step size of 50 seconds (Nyquist frequency 10^{-2} Hz). The algorithm provides a relative truncation error of $< 10^{-20}$ (more than 20 significant digits) in both satellite positions and velocities. Thereby, the range acceleration error is estimated to be $< 10^{-22}$ m/s² and well below 10^{-15} m/s². The roundoff error due to finite digits is approximately 10^{-33} m/s²/Hz^{1/2}, and no longer poses a limiting factor (see Fig. 1), which otherwise would overwhelm gravity-field signals in the case of double precision. To mitigate the low efficiency of quadruple-precision calculations, great effort was made in optimizing code execution to significantly reduce the run time. Other quadruple-precision orbit simulations can be found in, e.g., Refs. [28,29].

B. Detailed force models

As the satellites are drag-free controlled, we only consider pure freefall orbits of the TMs in order to focus on the gravitational perturbative effects. Excluding non-gravitational forces, the force models implemented are summarized in Table I. The types of gravity-field models are comparable with those used in the Earth's gravity field determination in satellite missions, such as GRACE [17,30] and GOCE [19].

The Solar System ephemeris uses DE430 [31] including all eight planets and the Moon. The effect from the main belt asteroids is estimated to not enter LISA's detection band [39], nor TianQin's due to the shorter arm length. Hence, they are not included in the simulation.

For the Earth's orientation, the International Astronomical Union (IAU) 2006 precession and IAU 2000A nutation models [32] are used with the help of the Standards Of Fundamental Astronomy (SOFA) software collection [40].

TABLE I. The list of force models implemented in the simulation.

Models	Specifications
Solar system ephemeris	JPL DE430 [31]
Earth's precession and nutation	IAU 2006/2000A [32]
Earth's polar motion	EOP 14 C04 [33]
Earth's static gravity field	EGM2008 ($n = 12$) [34]
Solid Earth tides	IERS (2010) [32]
Ocean tides	FES2004 ($n = 10$) [35]
Solid Earth pole tide	IERS (2010) [32]
Ocean pole tide	Desai (2003) [32]
Atmospheric tides	Biancale and Bode (2003) [36]
Moon's libration	JPL DE430 [31]
Moon's static gravity field	GL0660B ($n = 7$) [20]
Sun's orientation	IAU [37], Table 1
Sun's J_2	IAU [37], Table 1
Relativistic effect	post-Newtonian [38]

For the Earth's polar motion we adopt the IERS Earth Orientation Parameters (EOP) 14 C04 data series [33].

Earth's nonspherical static gravity field is provided by the EGM2008 model [34], following the recommendation of IERS (2010) [32]. The normalized spherical harmonic coefficients (\bar{C}_{nm} , \bar{S}_{nm}) are kept up to the 12th degree and order. High-degree terms decay rapidly with increasing radius as $1/r^{n+1}$. Our numerical tests and perturbation analysis show that the effect from the ninth-degree gravity field has already dropped below 10^{-15} m/s²/Hz^{1/2}. The contribution from the 12th degree sinks deeper to the level of 10^{-18} m/s²/Hz^{1/2}. Hence, we deem it safe to truncate at the degree and order 12.

Temporal variations of the Earth's gravity field are added as corrections to the spherical harmonic coefficients. To model the Earth's tidal effects, we have followed IERS (2010) [32] and taken into account solid Earth tides (anelastic), ocean tides, solid Earth pole tide, and ocean pole tide, as specified in Table I. The widely used ocean tide model FES2004 [35] includes long-period (Ω_1 , Ω_2 , S_a , S_{sa} , M_m , M_f , M_{lm} , M_{sqm}), diurnal (Q_1 , O_1 , P_1 , K_1), semi-diurnal ($2N_2$, N_2 , M_2 , S_2 , K_2), and quarter-diurnal (M_4) waves. The coefficients up to the degree and order ten are used. Additionally, atmospheric tides are incorporated, though their effect is small compared to the solid Earth and ocean tides. The associated model [36] consists of the diurnal and semidiurnal waves S_1 and S_2 in the highest frequency constituents. The correction is made up to the degree eight and order five. The nontidal temporal gravity changes have been estimated to be orders of magnitude smaller than the static gravity [41], and will be discussed elsewhere.

The Moon's liberation varies by about $\pm 8^\circ$, and is provided by DE430 [31]. For the Moon's static gravity field, we use GL0660B [20] up to the degree and order seven, and the effect of the seventh degree and order alone is below 10^{-20} m/s²/Hz^{1/2}. The model was obtained from the Gravity Recovery and Interior Laboratory (GRAIL) mission [20] with improved low-degree harmonics. The lunar tide is not included, since the effect is quite small and (semi)monthly periodic, and hence out of the detection band, owing to the Moon's tidal locking with the Earth. The

TABLE II. Initial orbital elements of the TianQin constellation in the J2000-based Earth-centered equatorial coordinate system at the epoch 6 June, 2004, 00:00:00 UTC for evaluation purposes. Here a denotes the semimajor axis, e the eccentricity, i the inclination, Ω the longitude of ascending node, ω the argument of periapsis, and ν^{ini} the true anomaly.

	a	e	i	Ω	ω	ν^{ini}
SC1	100000.0 km	0	74.5°	211.6°	0°	30°
SC2	100009.5 km	0	74.5°	211.6°	0°	150°
SC3	99995.0 km	0	74.5°	211.6°	0°	270°

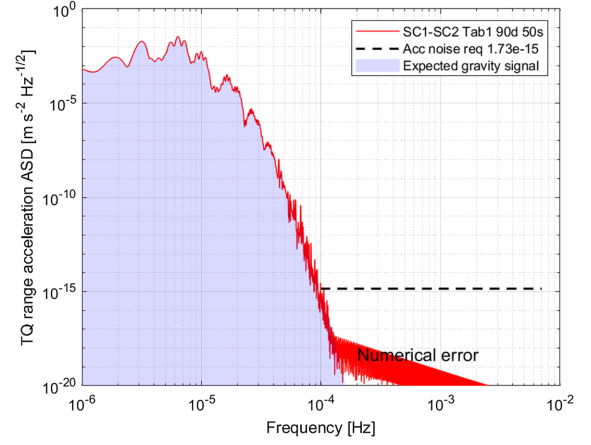


FIG. 2. Range acceleration ASD of two TianQin satellites SC1 and SC2, calculated in quadruple precision with the models of Table I and step size 50 s using 90 days of data. The orbital period 3.6 days corresponds to 3.2×10^{-6} Hz. The plots for SC1-SC3 and SC2-SC3 are nearly identical to the one shown above.

values of the Sun's oblateness J_2 and orientation are taken from Ref. [37] (see Table 9 in also Ref. [31]). Moreover, the relativistic effect is added as post-Newtonian correction terms to the equations of motion [38]. The effect is slowly varying and expected to be outside the detection band.

C. Orbital parameters

The initial orbital parameters are given in Table II. The integration lasts for one observation window of 3 months [1], that is, from 6 June to 4 September, 2004 for 90 days, when the orbital plane is facing the Sun within $\pm 45^\circ$. The year 2004 is chosen without preference but to take advantage of the available EOP observation data, which is more accurate than predictions in the 2030s. Our tests have shown that the dominant spectral behavior does not depend on the specific year chosen.

To make the simulation more realistic, we use the optimized initial orbital elements in Table II that can meet TianQin's constellation stability requirement (e.g., the breathing angles within $60 \pm 0.1^\circ$) for 3 months [10,11]. The optimization removes linear drift in the arm lengths and breathing angles, and prevents the nearly equilateral-triangle constellation from having severe distortion. The initial eccentricities are set to zero to keep the orbits almost circular. Note that even if one starts with less optimized initial orbital elements (e.g., the nominal values, $a = 10^5$ km, etc.), the dominant spectral behavior of 3 months (cf. Fig. 2) will be unaffected.

IV. SPECTRAL RESULTS

It should be emphasized that the purpose of this work is to determine the frequency-domain effects (especially $> 10^{-4}$ Hz) of various gravity disturbances on the range acceleration observable, and it concerns less about the

absolute accuracy of an integrated orbit, which may drift away from true values over long time scales outside the frequency band of interest.

A. Total effect

The overall result of the range acceleration ASD is presented in Fig. 2 for the arm SC1-SC2 using the models of Table I assembled together in the simulation. The plots for the other two arms severely overlap with the first one, and hence they are not presented for clarity.

In the frequency domain, the gravity field signals are dominating below 10^{-4} Hz, and roll off rapidly in amplitude toward high frequencies, and intersect with the lower end of the range acceleration noise requirement at 1×10^{-4} Hz. The steep falloff roughly follows a power law of $\sim 1.7 \times 10^{-15} \text{ m/s}^2/\text{Hz}^{1/2} \times (0.1 \text{ mHz}/f)^{24}$ near $f = 1 \times 10^{-4}$ Hz. The plot demonstrates that the effect of the gravity-field models in Table I does not enter the detection band $> 10^{-4}$ Hz. Note that the slanted part of the ASD curve ($< 10^{-17} \text{ m/s}^2/\text{Hz}^{1/2}$ and $> 10^{-4}$ Hz, marked by “Numerical error” in Fig. 2) is an artifact of the numerical interpolation of the EOP data.

The frequency-domain behavior somewhat resembles that in the intersatellite laser ranging measurement result of the GRACE Follow-On mission [18], which also shows a steep falloff, but at a higher frequency ($\sim 4 \times 10^{-2}$ Hz) because of its low orbital altitude of approximately 500 km.

B. Effect breakdown

Now we examine various contributions to the total range acceleration ASD of the arm SC1-SC2. The result is presented in Fig. 3.

The Earth's nonspherical static gravity field with degrees $n \geq 3$ dominates above 5×10^{-5} Hz in the total ASD, indicated by the overlapping of the blue and red curves. The effect decreases rapidly toward high frequencies and

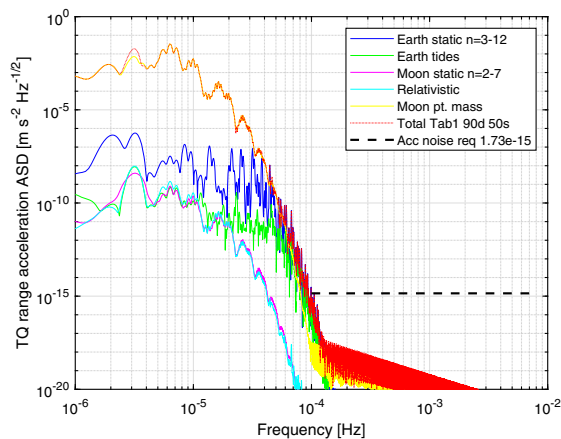


FIG. 3. Components of the range acceleration ASD of two TianQin satellites SC1 and SC2. The total ASD in Fig. 2 is duplicated as the dotted red curve for comparison.

impinges on the noise requirement at 10^{-4} Hz. At the high altitude of TianQin, high-degree harmonics are effectively attenuated.

The contribution from the Moon's nonspherical static gravity field ($n \geq 2$) is minute and only sticks out in the low-frequency region. One may have expected this since the Moon is a slowly rotating body. The same argument also justifies the omission of the lunar tides in the simulation. Nevertheless, the Moon's point mass and its orbital motion play an important role, largely accounting for the total ASD below 4×10^{-5} Hz.

The effects of relativity and Earth's tidal gravity field (solid Earth, oceanic, pole, and atmospheric, cf. Table I) are considerably smaller than the total effect, and both peak at low frequencies away from the detection band. These low-frequency disturbances show no significant coupling into high frequencies, and do not induce pronounced range acceleration response above 10^{-4} Hz.

C. Model errors

The models inevitably contain errors. A straightforward way to estimate their effect is to determine whether discrepancies between different models can significantly alter the spectral result in Fig. 2.

For a cross-check, we test another set of gravity-field models shown in Table III, where several replacements are made compared to Table I. The substitute models are deemed less accurate than the corresponding, more recent ones in Table I, and thus can mimic model errors (see, e.g., Ref. [42]). In Fig. 4, both ASD results show good agreement with each other, and the difference $\Delta\dot{\rho}$ is well below the noise requirement. In addition, the spectral behavior above $10^{-15} \text{ m/s}^2/\text{Hz}^{1/2}$ is also confirmed by running the flight-qualified, open source program GMAT [43] in

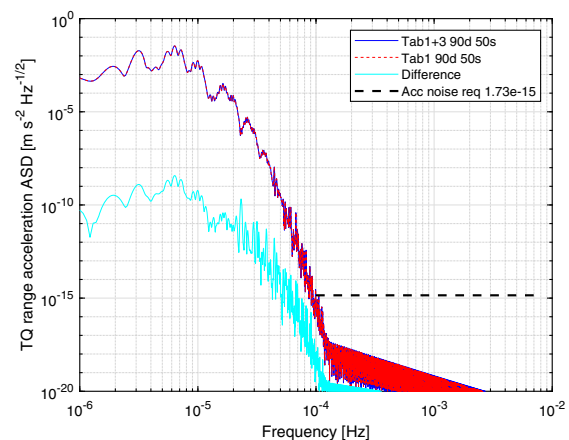


FIG. 4. Range acceleration ASD of two TianQin satellites SC1 and SC2 using the models of Table III for replacement for Table I (Tab1 + 3, blue). The ASD in Fig. 2 is duplicated as the dashed red curve (Tab1) for comparison. The ASD of their difference $\Delta\dot{\rho}$ is marked by the cyan curve.

TABLE III. List of replacement force models for Table I used for spectrum comparison.

Models	Specifications
Solar system ephemeris	JPL DE405 [44]
Earth's precession and nutation	IAU 1976/1980 [38]
Earth's static gravity field	EGM96 ($n = 12$) [45]
Moon's libration	JPL DE405 [44]
Moon's static gravity field	LP165P ($n = 7$) [46]

double precision. Hence, the overall frequency-domain behavior appears to be robust, which instills more confidence in the results.

V. CONCLUSION

The TianQin mission, to be deployed in a high Earth orbit, shares technological similarities with low-Earth gravimetry missions using satellite-to-satellite tracking. They diverge on a key point that the Earth's gravity-field signals targeted in gravimetry missions become environmental noise in TianQin's GW detection. Hence, TianQin must keep a safe distance from the Earth by flying high enough, so as to push the Earth's gravity-field interference out of the detection band. This work has been devoted to evaluating and examining this type of effect, and two main conclusions can be drawn here.

- (1) With the orbital radius of 10^5 km for TianQin, the current models show that the effect of the Earth-Moon's gravity field dominates at low frequencies, and that the amplitude rolls off rapidly toward high frequencies and intersects with the range acceleration noise requirement ($\sqrt{2} \times 10^{-15}$ m/s²/Hz^{1/2}) at 10^{-4} Hz, right on the lower end of the preliminary detection band. To provide more context, the gravity-field signals from GRACE-FO laser ranging interfer-

ometry along a ~ 200 km baseline fall off at about 4×10^{-2} Hz [18] with an orbital altitude of ~ 500 km.

- (2) The high-precision numerical simulations help to rule out the majority of the perturbing gravity sources for TianQin, including the Sun's point mass and its J_2 , the Solar System planets' point masses (under their orbital motion), the Earth's static gravity (with its rotation), the Earth's tidal gravity changes (solid Earth, oceanic, pole, and atmospheric), the Moon's static gravity, the relativistic effect, etc. (cf. Table I). These effects are slowly varying, do not enter the detection band, and present no show-stoppers for TianQin. The Newtonian gravity-field environment at a distance of 10^5 km from the Earth is expected to be fairly "quiet" for TianQin.

The results can provide useful input and guidelines for several aspects of the mission concept studies, such as orbit selection, noise reduction, and data processing. For future works, further refined gravity models will be explored to identify other possible noise sources. On another note, the strong low-frequency gravity-field signals ($< 10^{-4}$ Hz) illustrated in Fig. 2, which carry long-wavelength gravity information, may find potential applications in geodesy and geophysics [47]. This may help to enrich TianQin's secondary science output.

ACKNOWLEDGMENTS

The authors thank Qiong Li, Xiaoli Su, Fan Yang, Hao Zhou, Vitali Müller, Gerhard Heinzl, Bo Xu, Shuai Liu, Yi-Ming Hu, Hui-Zong Duan, Lin Zhu, Jinxiu Zhang, Cheng-Gang Shao, Shan-Qing Yang, Hsien-Chi Yeh, and anonymous referees for helpful discussions and comments. The work is supported by the National Key R&D Program of China (No. 2020YFC2201202). X. Z. is supported by NSFC Grant No. 11805287.

-
- [1] J. Luo *et al.*, *Classical Quantum Gravity* **33**, 035010 (2016).
 - [2] NASA Gravitational-Wave Mission Concept Study Final Report (2012), https://pcos.gsfc.nasa.gov/physpag/GW_Study_Rev3_Aug2012-Final.pdf.
 - [3] B. Hiscock and R. W. Hellings, *Bull. Am. Astron. Soc.* **29**, 1312 (1997).
 - [4] R. W. Hellings, S. L. Larson, S. Jensen, C. Fish, M. Benacquista, N. Cornish, and R. Lang, A Low-Cost, High-Performance Space Gravitational Astronomy Mission (2011), <https://pcos.gsfc.nasa.gov/studies/rfi/GWRFI-0007-Hellings.pdf>.
 - [5] M. Tinto, D. DeBra, S. Buchman, and S. Tilley, *Rev. Sci. Instrum.* **86**, 014501 (2015).
 - [6] S. T. McWilliams, [arXiv:1111.3708](https://arxiv.org/abs/1111.3708).
 - [7] S. Kawamura *et al.*, *Int. J. Mod. Phys. D* **27**, 1845001 (2018).
 - [8] W. M. Folkner, F. Hechler, T. H. Sweetser, M. A. Vincent, and P. L. Bender, *Classical Quantum Gravity* **14**, 1405 (1997).
 - [9] M. Tinto and S. V. Dhurandhar, *Living Rev. Relativity* **17**, 6 (2014).
 - [10] B. Ye, X. Zhang, M. Zhou, Y. Wang, H. Yuan, D. Gu, Y. Ding, J. Zhang, J. Mei, and J. Luo, *Int. J. Mod. Phys. D* **28**, 1950121 (2019).
 - [11] Z. Tan, B. Ye, and X. Zhang, *Int. J. Mod. Phys. D* **29**, 2050056 (2020).
 - [12] S. Barke, Ph.D. dissertation, Gottfried Wilhelm Leibniz Universität Hannover, 2015.

- [13] R. Weiss and D. Muehlner, Quarterly progress report, Research Laboratory of Electronics (MIT) **105**, 54 (1972).
- [14] J. Harms, *Living Rev. Relativity* **22**, 6 (2019).
- [15] G. Nelemans, *Classical Quantum Gravity* **26**, 094030 (2009).
- [16] P. Amaro-Seoane *et al.*, arXiv:1702.00786.
- [17] B. D. Tapley, S. Bettadpur, M. Watkins, and C. Reigber, *Geophys. Res. Lett.* **31**, L09607 (2004).
- [18] K. Abich *et al.*, *Phys. Rev. Lett.* **123**, 031101 (2019).
- [19] R. Floberghagen, M. Fehringer, D. Lamarre, D. Muzi, B. Frommknecht, C. Steiger, J. Piñeiro, and A. da Costa, *J. Geodes.* **85**, 749 (2011).
- [20] A. S. Konopliv, R. S. Park, D.-N. Yuan, S. W. Asmar, M. M. Watkins, J. G. Williams, E. Fahnestock, G. Kruizinga, M. Paik, D. Strelakov *et al.*, *J. Geophys. Res. Planets* **118**, 1415 (2013).
- [21] S. Liu, L.-X. Liu, Z.-B. Tan, Y.-M. Hu, X. Zhang, J. dong Zhang, J. Zhang, J. Mei, and J. Luo, Internal technical report (unpublished) (2019).
- [22] L.-F. Lu, Y. Liu, H.-Z. Duan, Y.-Z. Jiang, and H.-C. Yeh, *Plasma Sci. Technol.* **22**, 115301 (2020).
- [23] W. Su, Y. Wang, Z.-B. Zhou, Y.-Z. Bai, Y. Guo, C. Zhou, T. Lee, M. Wang, M.-Y. Zhou, T. Shi *et al.*, *Classical Quantum Gravity* **37**, 185017 (2020).
- [24] L.-F. Lu, W. Su, X. Zhang, Z.-G. He, H.-Z. Duan, Y.-Z. Jiang, and H.-C. Yeh, *J. Geophys. Res.: Space Phys.* **126**, e2020JA028579 (2021).
- [25] V. Müller, Ph.D. dissertation, Gottfried Wilhelm Leibniz Universität Hannover, 2017.
- [26] M. Armano *et al.*, *Phys. Rev. Lett.* **116**, 231101 (2016).
- [27] P. J. Prince and J. R. Dormand, *J. Comput. Appl. Math.* **7**, 67 (1981).
- [28] C. McCullough, S. Bettadpur, and K. McDonald, *J. Spacecraft Rockets* **52**, 766 (2015).
- [29] F. Wöske, T. Kato, M. List, and B. Rievers, *Adv. Astr. Sci.* **158**, 2445 (2016).
- [30] B. D. Tapley, S. Bettadpur, J. C. Ries, P. F. Thompson, and M. M. Watkins, *Science* **305**, 503 (2004).
- [31] W. M. Folkner, J. G. Williams, D. H. Boggs, R. S. Park, and P. Kuchynka, IPN Progress Report No. 42-196, Jet Propulsion Laboratory, 2014.
- [32] G. Petit and B. Luzum, Bureau International Des Poids Et Mesures Sevres (France) Technical Report No. 36, 2010.
- [33] <http://hpiers.obspm.fr/iers/eop/eopc04/>.
- [34] N. K. Pavlis, S. A. Holmes, S. C. Kenyon, and J. K. Factor, *J. Geophys. Res.* **117**, B04406 (2012).
- [35] F. Lyard, F. Lefevre, T. Letellier, and O. Francis, *Ocean Dyn.* **56**, 394 (2006).
- [36] R. Biancale and A. Bode, STR 06/01, GeoForschungs Zentrum Potsdam (2006).
- [37] B. A. Archinal, M. F. A'Hearn, E. Bowell, A. Conrad, G. J. Consolmagno, R. Courtin, T. Fukushima, D. Hestroffer, J. L. Hilton, G. A. Krasinsky *et al.*, *Celest. Mech. Dyn. Astron.* **109**, 101 (2011).
- [38] D. D. McCarthy, Central Bureau of IERS—Observatoire de Paris Technical Report No. 21, 1996.
- [39] D. Bronicki, B. Bolen, and S. Larson, *Poster in the 12th International LISA Symposium* (2018).
- [40] <http://www.iausofa.org/>.
- [41] T. Gruber, J. L. Bamber, M. F. P. Bierkens, H. Dobslaw, M. Murböck, M. Thomas, L. P. H. Van Beek, T. van Dam, L. L. A. Vermeersen, and P. N. A. M. Visser, *Earth Syst. Sci. Data* **3**, 19 (2011).
- [42] B. D. Loomis, R. S. Nerem, and S. B. Luthcke, *J. Geod.* **86**, 319 (2012).
- [43] <http://gmtcentral.org>.
- [44] E. M. Standish, Jet Propulsion Laboratory Report No. IOM 312.F-98-048, 1998.
- [45] F. Lemoine *et al.*, NASA Technical Paper No. NASA/TP-1998-206861, 1998.
- [46] A. S. Konopliv, S. W. Asmar, E. Carranza, W. L. Sjogren, and D. N. Yuan, *Icarus* **150**, 1 (2001).
- [47] L. Jiao and X. Zhang, *Poster in 2019 Annual Conference of HUST CGE and SYSU TRC* (2020).